Res. Rep. Fac. Eng. Mie Univ., Vol. 22, pp. 11−23 (1997)

Original Paper

Influence of Metallurgical Factors on Temper Embrittlement in HAZ of Cr–Mo Steel

Koreaki TAMAKI, Hiroshi KAWAKAMI, Masatoshi KOJIMA
Yoshihiro AKAZAKI, Kenji NOMOTO
(Department of Mechanical Engineering)

(Received September 12, 1997)

Abstract

Five types of temper embrittlement arose in HAZ of Cr–Mo steel in the temperature range of 775K to 875K. The metallurgical factors affecting those types of embrittlement were discussed from the view point of the precipitation and growth of carbide, the size and shape of ferrite grains and the segregation of impurity elements. The first and the second types of embrittlement are induced by the secondary hardening brought about by the coherent precipitation of M_2C. The third type is induced by the segregation of impurity elements in the grain boundary. The fourth type is possibly induced by the coarsening of M_2C and M_7C_3. The fifth type is induced mainly by the coarsening of ferrite grains.

Key words: Cr–Mo steels, heat affected zone, temper embrittlement, growth of carbide particles, growth of ferrite grains, segregation of impurities.

1. Introduction

The welded zone produced by arc welding is composed of the weld metal, the heat affected zone (HAZ) and base metal as shown in Fig.1. The heat of welding is given to the HAZ and it flows immediately to the base metal. The HAZ is cooled as rapidly as the case of quenching as shown in Fig.2, and hence, its microsturcture is composed of martensite and bainite. The

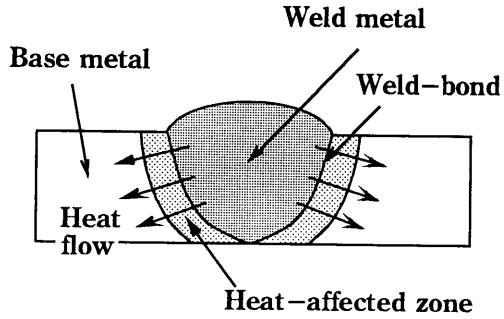

Fig.1 Welded zone produced by arc welding.

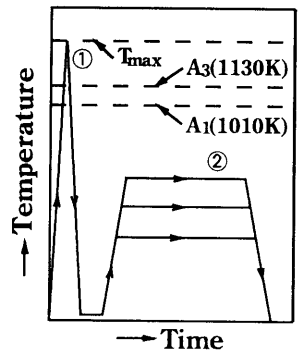

Fig.2 Thermal cycles given to HAZ during and after welding, ①Welding, ②Tempering,

HAZ is then tempered when the welded constructions, such as boilors and pressure vessels are used in service at an elevated temperature (Fig.2). One of the unfavorable phenomenon observed in the HAZ of Cr–Mo steel is the temper embrittlement [1–3] arising after long–term tempering. The temper embrittlement is detected as the rise of transition temperature obtained by Charpy impact test [5–8]. The authors have made a series of investigation on this phenomenon in Cr–Mo steels, and pointed out that there existed five types of embrittlement in the temperature range of 775K to 975K [4–9]. They believed that each of these types will be closely related to the metallurgical factors. In this research, the major metallurgical factors, such as the precipitation of carbide, the growth of ferrite grains and the segregation of impurity elements were discussed on the basis of the experimental results of the authors.

2. Time–temperature range where temper embrittlement arises

The time –temperature ranges where the first to fifth types of embrittlement and the de–embrittled state arise were shown in a diagram of Fig.3 [6,9]. In this diagram, 1/T and log t are taken in the main vertical and horizontal axes with normal spacing, the tempering temperature T(K) and the time t (hr)are shown in the corresponding positions of sub–axes. The diagram of Fig.3 informs the following facts: (1)The third type of embrittlement begins to appear at cd line before the second type disappears at a'b' line. The former survives after the fourth type begins to appear at ef line. (2)The third and the fourth types are alive below the critical temperatures of cc' and eg. (3)The fifth type appears above the critical temperature of hi. It will arise in a wide temperature range below A_1 temperature. (4)The specimen becomes the de–embrittled state after the second type of embrittlement disappears and before the fourth or the fifth type begins to appear.

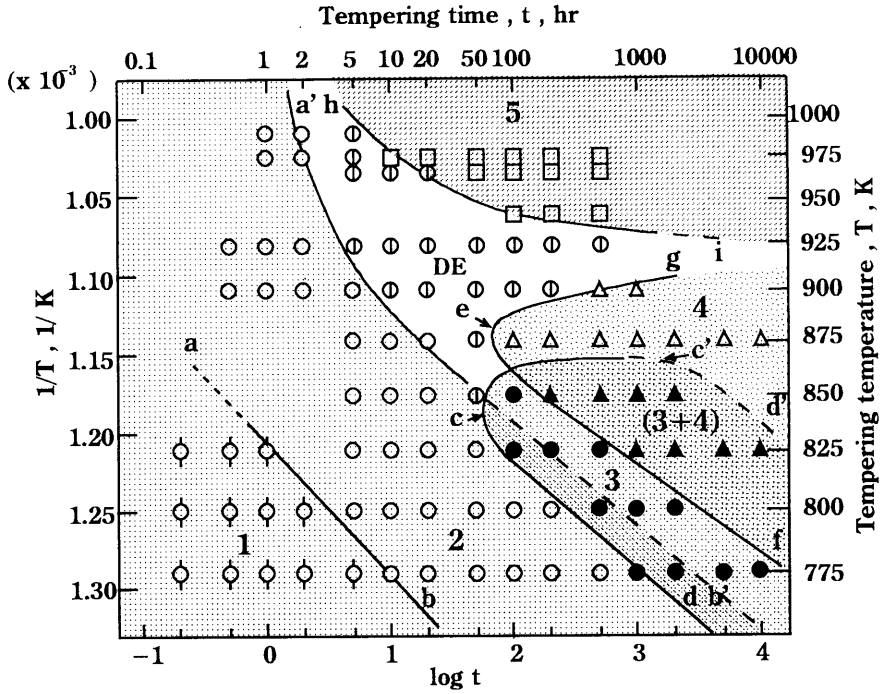

Fig.3 Tempering temperature–time fields where five types of temper embrittlement arise in 2 1/4Cr–1Mo steel; Marks show the specimen in the embrittled state of; ϕ first type, ○ second type, ● third type, △ fourth type, ▲ third and fourth type, □ fifth type, ⊕ de–embrittle state.

3. Behavior of carbide during tempering

3.1 General process of carbide phase change during tempering

Following carbide phase chanege will be expected during tempering of Cr–Mo steel[10].

(1)The steel in the quenched state has the microstructure of bainite and martensite.

(2)ε carbide ($Fe_{2.4}C$) precipitating in martensite and bainite is cementite (Fe_3C) in the earlier stage of tempering.

(3)In the next stage of tempering, cementite is replaced by molybdenum carbide, Mo_2C and chromiun carbide, Cr_7C_3.

(4)Mo_2C is informed with two stages; in the first stage, a fine platelet precipitate is formed keeping a coherency with the ferrite matrix, and in the second stage, a three–dimensional precipitate is formed losing the coherency with the matrix.. A significant increase of hardness is observed in the first stage of precipitation.

(5)It has been beleved that Cr_7C_3 nucreats in pre–existing cementite and grows consuming the latter as shown in Fig.4(a). In this case, therefore, the increase of hardness observed in case of the precipitation of Mo_2C (separate nucleation; Fig.4(b)) does not occur.

(6)In the final tempering stage, both Mo_2C and Cr_7C_3 are disappear to produce a chromium carbide, $Cr_{23}C_6$ or molybdenum rich carbide, $Fe_{21}Mo_2C_6$.

Metallic atom (iron, chromium or molybdenum) in the carbide phase of Fe_3C, Mo_2C, Cr_7C_3, $Cr_{23}C_6$ or $Fe_{21}Mo_2C_6$ can be replaced considerablly by other atoms, and hence, each carbide phase is expressed by the generallized formula of M_3C, M_2C, M_7C_3 or $M_{23}C_6$, in which "M" represents Fe, Cr or Mo as shown in Table 1. $Cr_{23}C_6$ and $Fe_{21}Mo_2C_6$ was beleved to form solid solution in each other in Cr–Mo steels [10], and therefore, a single generallized formula of "$M_{23}C_6$" was adopted for those carbide phases.

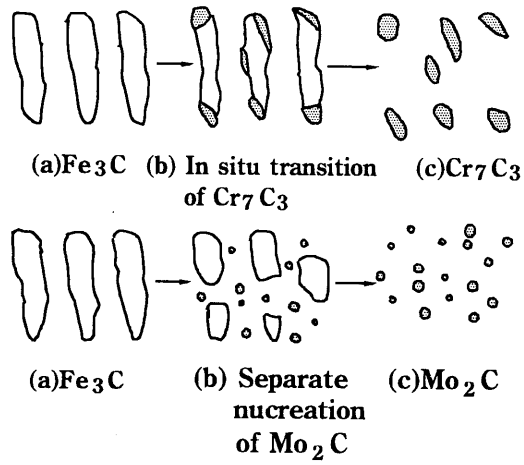

Fig.4 Different nucreation systems of Cr_7C_3 and Mo_2C.

Table 1 Carbide types present in Cr–Mo steel.

Fundamental formura	Generalized formura	Metals, M*
Fe_3C	M_3C	Fe, Cr, Mo
Cr_7C_3	M_7C_3	Cr, Mo, Fe
$Cr_{23}C_6$ $Fe_{21}Mo_2C_6$	$M_{23}C_6$	Cr, Mo, Fe

*** Arranged in the order of increasing concentration.**

3.2 Coherent precipitation of M2C

(1) Preparation of HAZ specimen and measurement of hardness

The first stage of precipitation (the coherent precipitation) of M2C was detected in this research by the measurement of hardness.

2 1/4Cr–1Mo steel of the chemical composition of Table 2 was used. The microstructure of HAZ (in this case 75% bainite and 25% martensite) was reproduced in a steel plate of 7 x 13mm in cross-section by using a weld-thernal simulator. This synthetic HAZ specimen was tempered at 775 to 975K for up to 10000 hours.

Table 2 Chemical composition of 2 1/4Cr–1Mo Steel(wt%).

C	Si	Mn	P	S	Cr	Mo	As	N	Al_{sol}
0.14	0.16	0.56	0.006	0.002	2.17	0.90	0.004	0.0032	0.017

The Vickers hardness of each specimen was measured at room temperature.The hardness test was made with the load of 500N on the center portions of the specimen.

(2)Hardness change of the specimen

The changes in hardness with an increasing tempering time at 775K to 825K are shown in Fig.5 for the specimens tempered at 825K. The dotted line attached to the hardness curve shows an assumed hardness of the specimen in the non-hardened state. The increase of hardness is ob-

served in the time ranges in which the first type (left side of S2), the second type (S2 to S3) and the third type of embrittlement (right side of S3) occur. The increment of hardness, ΔH in the figure was measured for all the specimens in Fig.3 as shown in Fig.6. In the temperature range

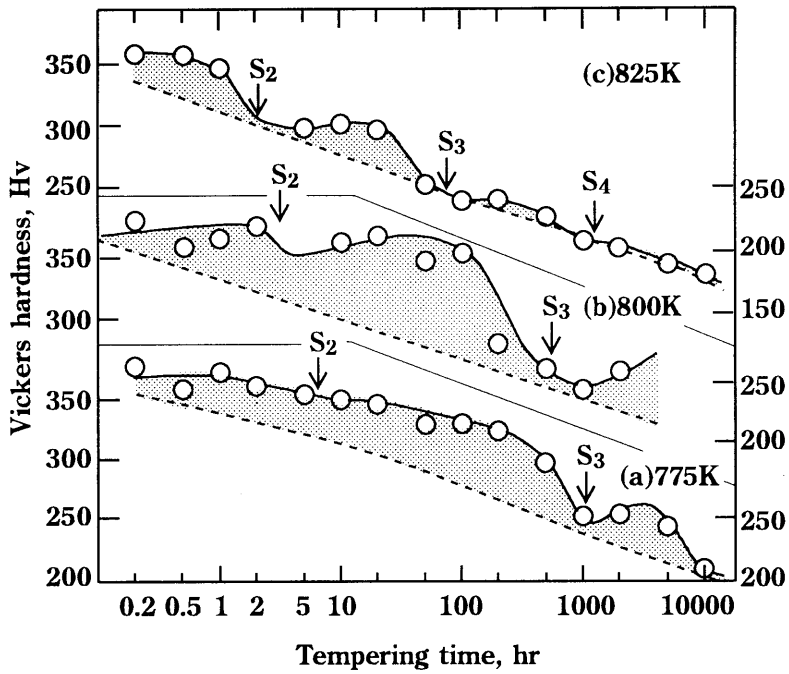

Fig.5 Change of hardness with the lapse of tempering time at 775K to 825K.

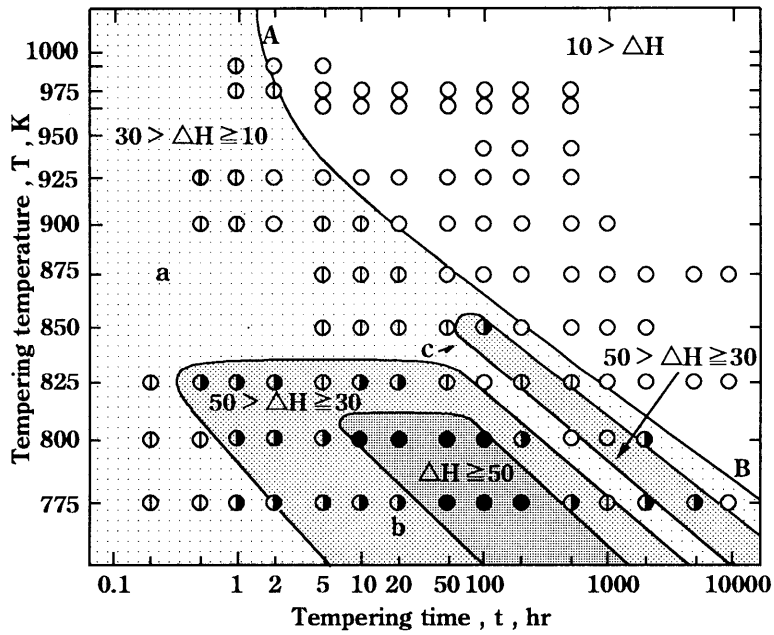

Fig.6 Increment of hardness ΔH induced by secondary hardening shown in temparing temperature–time diagram;
● ΔH ≧ 50, ◑ 50 > ΔH ≧ 30, ⦶ 30 > ΔH ≧ 10, ○ 10 > ΔH.

below 875K, the ΔH increases to the top hill (ΔH≥ 50) around 775K for 100hr and then decreases passing through the second hill around 800K for 1000hr. In the temperature range above 850K, the hill of large ΔH is not recognized. The ΔH decreases when the tempering time exceeds AB line in the figure. Those results suggest following facts in reference to the embrittlement diagram of Fig.3. (1)The secondary hardening induced by the coherent precipitation of M_2C occurs most significantly in the time-temperature range in which the second type of embrittlement arises. (2)A significant secondary hardening is also occurs in the time-temperature ranges in which the final part of the first type and beginning part of the third type arise. (3)The secondary hardening does not occur in the ranges in which the fourth type and the fifth type of embrittlement arise as well as the de-embrittled state appears.

3.3 Microscopic change of M_2C particles

(1) Method of measuring carbide particles

M_2C particles which were grew up as large as the three-dimensional size was observed by an SEM. The numbers of carbide particles in an unit area were counted by the following method. An outline enclosing a squar of 5 x 5 μm was drawn at random on an SEM-microphotograph. The numbers of carbide particles locating in this squar were counted.

Average size of carbide particles was measured by the following procedure. One SEM microphotpgraph was selected at random. Carbide particles exhibit a spherical and an elongate shapes; the diameter and the length respectively, were measured for each of these particles in the photo print. Measurements were made separately on the particles locating in ferrite matrix and that in the grain boundaries of prior-austenite.

(2)Number and size of carbide particles

The number, N and the size of carbide particles are shown in the time-temperature diagrams as Fig.7 and 8. The S in Fig.8 represents the mean of sizes of the particles locating in ferrite matrix and that in grain boundary. The tempering time-temperature field can be divided

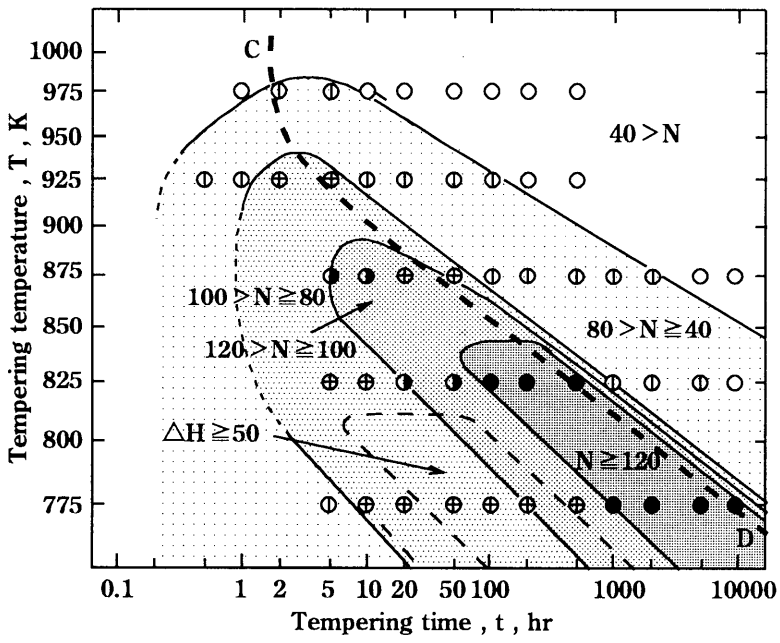

Fig.7 Numbers of carbide particles in 5 μm square, N shown in the tempering temperature-time diagram; CD line: beginning of the growth of carbide particles; ● N≧120, ◑ 120>N≧100, ⊕ 100>N≧80, ◌ 80>N≧40, ○ 40>N.

into two regions by the line CD. In the region left side of CD, the N increases, and hence, the S decreases with an increasing tempering time; it means that pre-existing coarse carbide particles were replaced by fine ones. The former will be cementite, M_3C and the latter will be M_2C. In the

region right side of CD, the N decreases, and the S increases with an increasing tempering time ; that is the particles of M_2C and M_7C_3 grow significantly when the specimen is tempered to this region.

The third type of embrittlement (Fig.3) arises in the temperature-time range where the particle size, S is smallest. The fourth type arises in the range where the S is larger (around 0.1μm). The fifth type appears in the range where the S is largest (around 0.4μm).

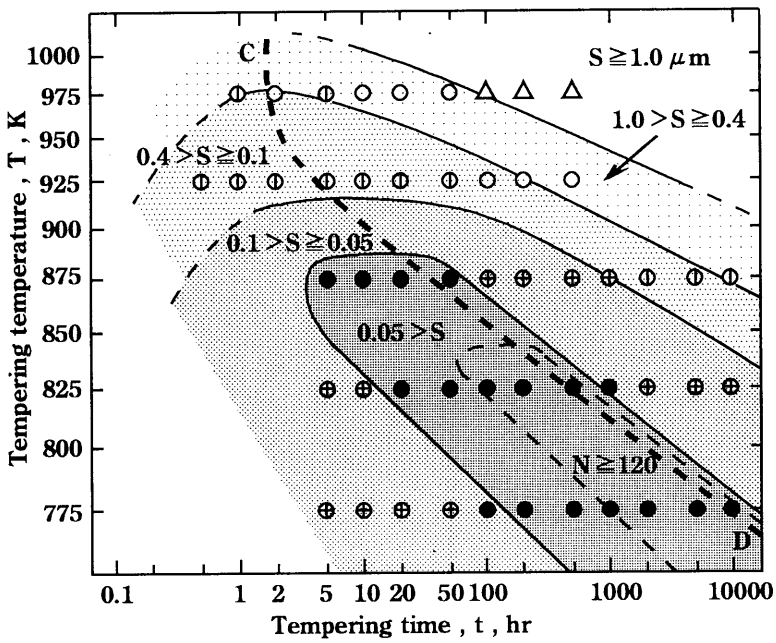

Fig.8 Mean particle size of carbide, S shown in tempering temperature-time diagram; ● 0.05>S, ⊕ 0.1>S≧0.05, Φ 0.4>S≧0.1, ○ 1.0>S≧0.4, △ S≧1.0 μm.

3.4 Change of carbide type

(1)Determination of carbide type

Carbide particles in steel specimen were extracted electrolytically by using the apparatus shown in Fig.9. 1L of 0.5N HCl was used as the electrolyte; the current density was 10mA/cm^2. The electrolysis was continued for 100 hours by replacing the electolyte with the fresh one for every 24 hours. 0.26g of carbide was extracted as the anode residue.

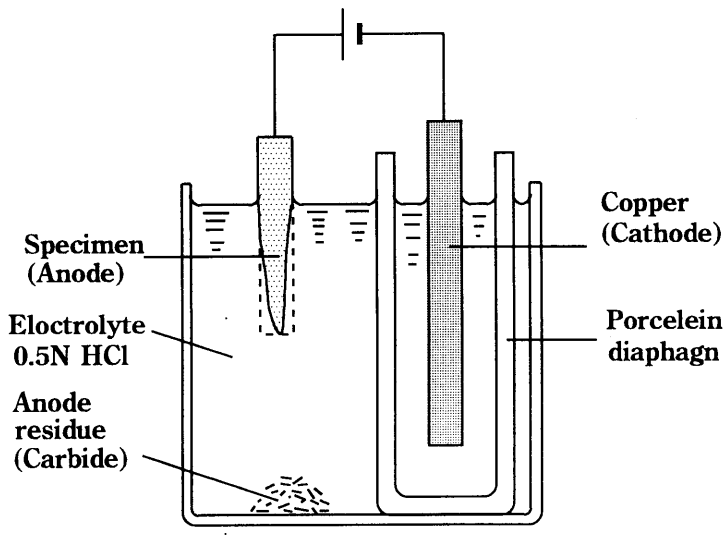

Fig.9 Apparatus for electrolytic extraction of carbide.

The residue was moved to a glass cylinger together with the electrolyte in the bottom portion. The residue was washed by water by repeating the decantation. It was washed finally by ethyl alcohl. The residue was filtrated through a glass-paper filter.

The residue together with the filter was attached to a glass plate of the X-ray diffraction apparatus. X-ray diffraction with a chromium target was carried out for identify the type of carbide. The data cards published by JCPDS [11] were used as the standard diffraction patterns.

(2) Carbide types in the specimens

The change of the types of carbide with progressing tempering is shown in the time-temperature diagram of Fig.10. This figure informs the following facts.

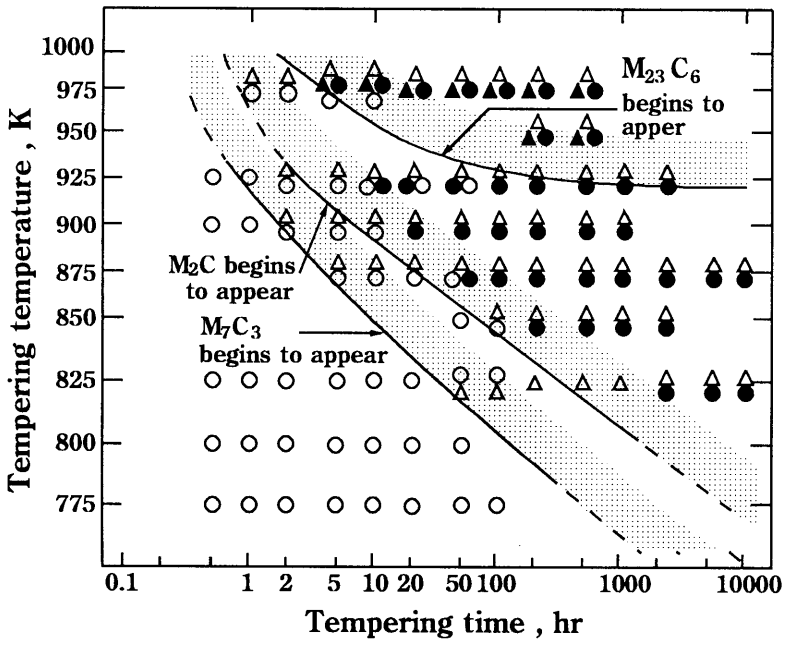

Fig.10 Crabide types shown in the tempering temperature-time diagram;
○ M_3C, ● M_2C, △ M_7C_3, ▲ $M_{23}C_6$;
The mark are arranged in the order of quantity of carbide: large (top), medium (left), and small (right), smallest(bottom).

(i)The carbide types present in the temperature range below 925K are M_2C and M_7C_3.

(ii)M_7C_3 is detected in the earlier time period of tempering than M_2C does. M_2C can be detected only when the specimens are tempered in the temperature-time range in which the M_2C particles begin to grow (right side of CD line of Fig.7 and 8).

(iii)$M_{23}C_6$ is detected in the temperature range above 925K.

(iv)M_2C and M_7C_3 continue to appear in the temperature range where the third and the fourth type arise.

(v)$M_{23}C_6$ other than M_2C and M_7C_3 appears in the temperature range where the fifth type of embrittlement arises.

4. Behavior of ferrite grain during tempering

4.1 Change in morphology of ferrite grains

The morphology of ferrite grains was observed by using an optical microscope. The microphographs of specimens tempered at 975K for 5, 50 and 500 hours and etched by 3% nital are shown in Fig.11. The martensite-lath structure which existed before the tempering transforms into the ferrite-lath structure by the tempering for 5 hours (Fig.11(a)). Each ferrite-lath joins together to form an elongated ferrite grain by the tempering for 50 hours (Fig.11(b)). An elongated ferrite grain grows joining the other grains and passing through the grain boundary of prior-austenite, as a result, a large polygonal ferrite grain is produced (Fig.11(c)).

4.2 Change in size of ferrite grains

The changes in the size parameter (the area, the length and the width) of ferrite grains with the lapse of tempering time at 975K are shown in Fig.12(b) and (c). The change of the size of ferrite grains corresponds well to that of vTr_{30} (Fig.12(a)) as follows. (a) The time periods at which the fifth type of embrittlement begins to appear and arises very significantly meet, respectively those at which the ferrite grains begins to grow and grows very intensively. (b)Ferrite grains become polygonal in shape by reducing its width and decreasing its length at the time

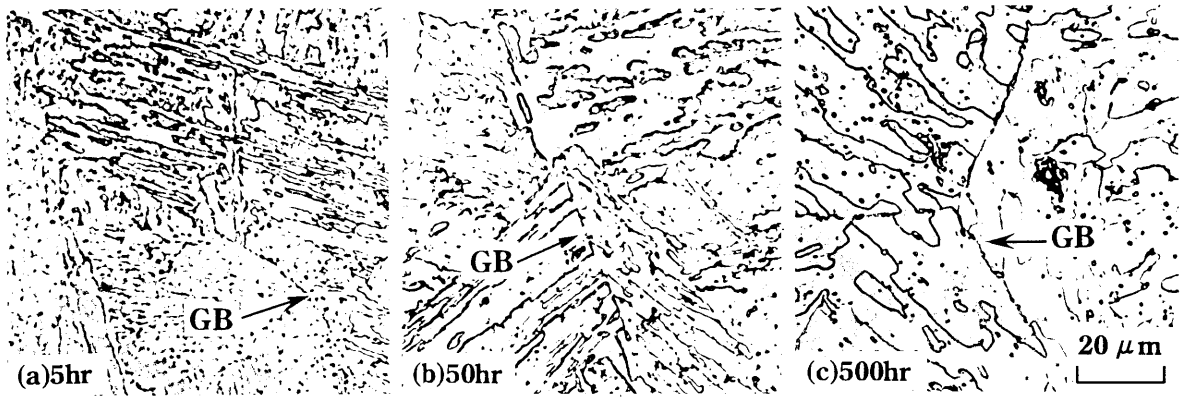

Fig.11 Change of morphorogy of ferrite grains with an increasing tempering time at 975K; GB: grain boundary of prior-austenite.

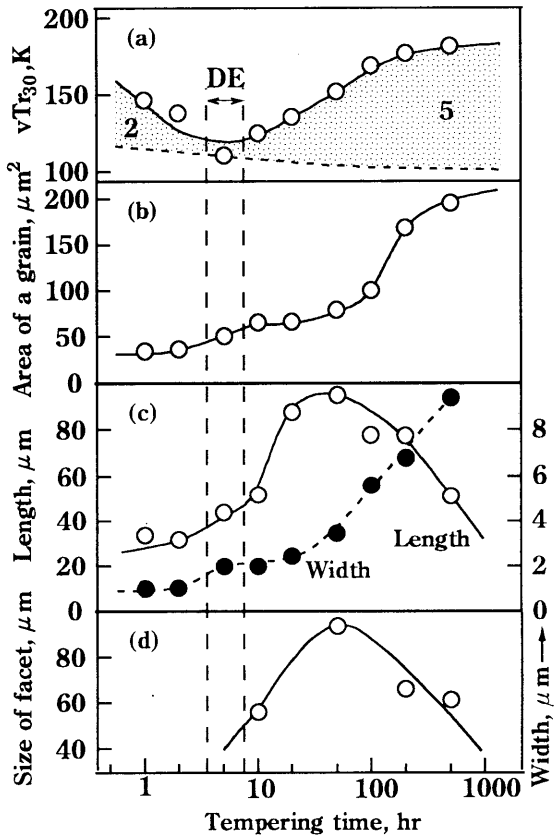

Fig.12 Change in size and shape of ferrite grains with an increasing tempering time at 975K and their effects on the fifth type of temper embrittlement.

when the embrittlement arises very intensively. That is, the original shape of ferrite, which succeeds the orientation of martensite-lath, is disappeared at this time period, and the ferrite grains grow freely in several direction.

4.3 Change in facet size

The specimens fractured at and near the transition temperature exhibit the mixed fractures of a cleavage and a dimple. The cleavage fracture is composed of small partitioned areas, "facet". The change in facet size with the lapse of tempering time is shown in Fig.12(d). This result informs that the facet size is same approximately as the length of the ferrite grains (Fig.10(c)).

5. Behavior of impurity elements during tempering

The specimen suffered from the third type of embrittlement is fractured at the grain boundary of prior-austenite as shown in Fig.13(a). In the time range in which this type of embrittlement arises (around 1000hr at 825K), the grain boundary will become weaker than the cleavage plane as shown in Fig.13(b). The cause of weakening the grain boundary will be the segregation of impurity elements.

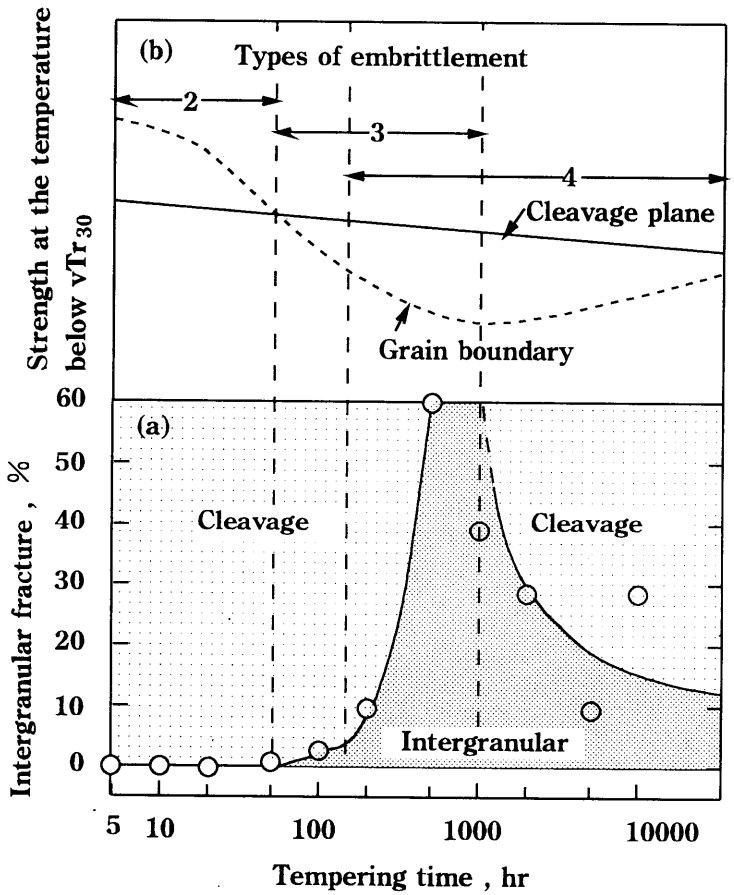

Fig.13 Interagranular fracture brought about by the decrease of grain boundary strength in the time range where the third type of embrittlement arises.

The impurity elements segragated in the grain boundary of prior-austenite were analyzed by an Auger electron spectroscopy(AES). The specimen suffered from the third type of embrittlement(tempered at 800K for 1000hours) was fractured in liquid nitrogen placed in an AES apparatus. The Auger spectra revealing the segregation of impurity elements are shown in Fig.14.

The segregation of nitrogen is observed other than the well-known impurity element, phosphorus. The segregation of phosphorus in the grain boundary was detected by EDX analysis on the cross-section of the same specimen. A precise point-counting method was applied to the microregion around a grain boundary.The segregation of phosphorus is confimed again by this method as shown in Fig.15.

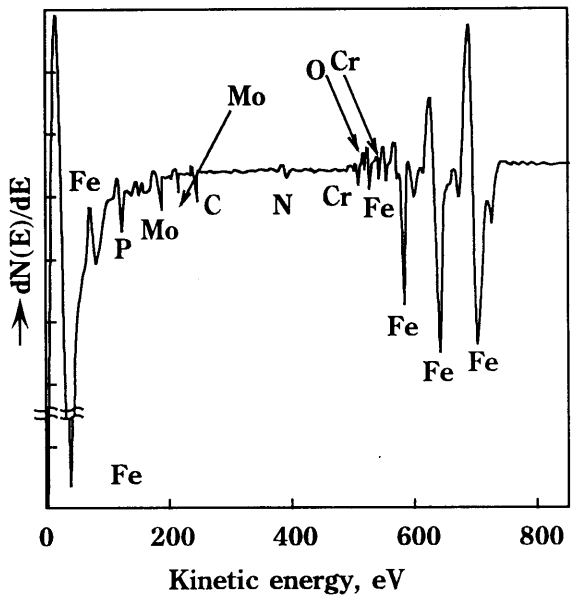

Fig.14 Auger spectra showing the segragation of impurities at grain boundary; specimen was suffered from the third type of embrittlement.

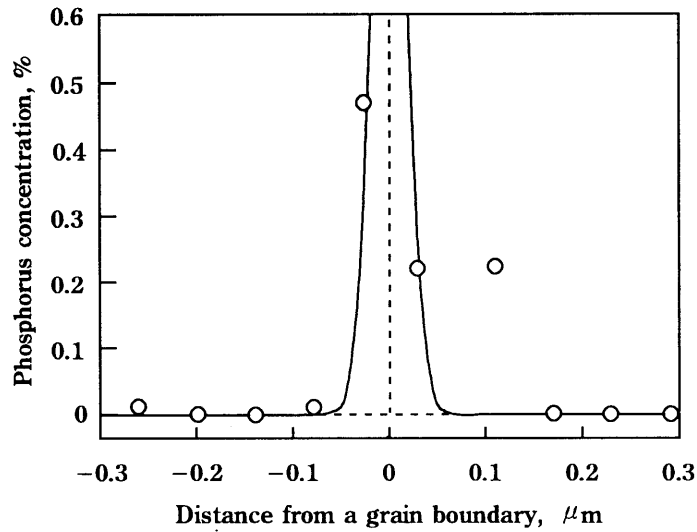

Fig.15 Phosphorus concentration in the grain boundary meaured by point counting method in EDX analysis; specimens was suuffered from the third type of embrittlement.

6. Influence of metallurgical factors on temper embrittlement

6.1 The first and the second types of embrittlement

The secondary hardening induced by the coherent precipitation of M_2C occurs most intensively when the second type of embrittlement arises (Fig.6). The secondary hardening occurs also when the first and the third types arise. Those results suggest that the hardening arising in ferrite matrix will be one of the major metallurgical factor to cause the first, the second and the third types of embrittlement.

6.2 The third type of embrittlement

The third type of embrittlement is accompanied generally by the intergranular fracture, and the impurity elements, such as phosphorus and nitrogen were concentrated in the grain boundary. This fact indicates that the third type of embrittlement is induced mainly by the segregation of those elements. The secondary hardening will assist the third type to occur as mentioned above.

6.3 The fourth type of embrittlement

Carbide particles grow very significantly in the time ranges where the fourth type of embrittlement arises (Fig.7 and 8). This result suggests that the major cause of fourth type of embrittlement will be the growth of carbide particles.

6.4 The fifth type of embrittlement

Very large ferrite grains are observed in the specimen suffered from the fifth type of embrittlemet, and the size of a ferrite grain is approximately same as that of a facet in the cleavage fracture (Fig.12). This fact suggests that the growth of ferrite grains will be the major factor to induce the fifth type of embrittlement.

7. Conclusions

The temper embrittlement arising in the HAZ of 2 1/4Cr–1Mo steel was discussed from the view point of the metallurgical causes. The results of discussions will be summerized as follows.

(1) The first and the second types of embrittlement are induced mainly by the secondary hardening brought about by the coherent precipitation of M_2C.

(2) The third type of embrittlement is induced mainly by the segregation of phosphorus and nitrogen. The secondary hardening will assist this type to occur.

(3) The fourth type of embrittlement is occured by a significant growth of carbide particles.

(4) The fifth type of embrittlement will be caused mainly by a significant growth of ferrite grains.

The authors wish to thank Dr. J.Suzuki, associate professor, and Mr. T. Niinomi, graduate student of Mie University for their cooperations to this research.

This research was supported by The Grant-in-Aid for Scientific Reseach of Ministry of Education and Culture, Japan.

References

[1]T. Takamatsu et al: Temper embrittlement characteristics of 2 1/4Cr-1Mo steel, Tetsu to Hagané, 67-1(1981),178-187 (in Japanese).

[2]F.C. Pickering et al: Materials Science and Technology, VCH Verlags, (1992), Vol.7, pp.170-171, 461-463.

[3]J.P. Naylor, M. Guttmann: Mechanism of upper-nose temper embrittlement in Mn-Ni-Mo A533 gr.B steel, Metal Science, 15-10(1981), 433-441.

[4]K.Tamaki, J.Suzuki, M.Tanaka:Stress-induced phosphorus-segregation and intergranular cracking in welded zone of 1Cr-1/2Mo steel, Res. Rep. Fac. Eng. Mie Univ., Vol.14(1989), 9-22.

[5]K.Tamaki, J.Suzuki, K. Ryouke: Factors affecting the temper embrittlement in HAZ of Cr-Mo steel, Res. Rep. Fac. Eng. Mie Univ., Vol.17 (1992), 21-36.

[6]K.Tamaki, J.Suzuki, H.Kawakami et al: Types of temper embrittlement in HAZ of Cr-Mo steel classified by tempering time, IIW Document IX-1745-94, (1994, Beijing, China).

[7]K.Tamaki, J.Suzuki H.Kawakami, K.Tanaka: SR embrittlement and temper embrittlement observed in HAZ of 2 1/4Cr-1Mo steel, Res. Rep. Fac. Eng. Mie Univ., Vol.20 (1995), 25-40.

[8]K.Tamaki, H.Kawakami, J.Suzuki et al:Temper embrittlement in HAZ of Cr-Mo steels arising in temperature range of stress relieving, IIW Document IX-1834-96 (1996, Budapest, Hungary).

[9]K.Tamaki, H.Kawakami, J.Suzuki et al: Influence of microstructure on embrittlement and loss of ductility in HAZ of 2 1/4Cr-1Mo steel, Res. Rep. Fac. Eng. Mie Univ., Vol.21 (1996), 11-25.

[10]K.Tamaki, J.Suzuki et al: Effect of carbides on reheat cracking sensitivity, Trans. Japan Welding Soc., 15-1(1984), 8-16.

[11]JCPDS International Centre for Diffraction Data: Selected Powder Diffraction Data for Metals and Alloys, (1978).